A new probabilistic seismic hazard assessment for greater Tokyo

Ross S. Stein[1], Shinji Toda[2], Tom Parsons[1] and Elliot Grunewald[1,3]

[1]U.S. Geological Survey, Menlo Park, California, USA
[2]Active Fault Research Center, AIST, Tsukuba, Japan
[3]Dept. of Geophysics, Stanford University, USA

Abstract. Tokyo and its outlying cities are home to one-quarter of Japan's 127 million people. Highly destructive earthquakes struck the capital in 1703, 1855 and 1923, the last of which took 105,000 lives. Fueled by greater Tokyo's rich seismological record but challenged by its magnificent complexity, our joint Japanese-U.S group carried out a new study of the capital's earthquake hazards. We used the prehistoric record of great earthquakes preserved by uplifted marine terraces and tsunami deposits (17 M~8 shocks in the past 7,000 years), a newly digitized dataset of historical shaking (10,000 observations in the past 400 years), the dense modern seismic network (300,000 earthquakes in the past 30 years), and Japan's GeoNet array (150 GPS vectors in the past 10 years) to reinterpret the tectonic structure, identify active faults and their slip rates, and estimate their earthquake frequency. We propose that a dislodged fragment of the Pacific plate is jammed between the Pacific, Philippine Sea and Eurasian plates beneath the Kanto plain on which Tokyo sits. We suggest that the Kanto fragment controls much of Tokyo's seismic behavior for large earthquakes, including the damaging 1855 M~7.3 Ansei-Edo shock. On the basis of the frequency of earthquakes beneath greater Tokyo, events with magnitude and location similar to the M~7.3 Ansei-Edo event have a ~20% likelihood in an average 30-yr period. In contrast, our renewal (time-dependent) probability for the great M≥7.9 plate boundary shocks such as struck in 1923 and 1703 is 0.5% for the next 30 yr, with a time-averaged 30-yr probability of ~10%. The resulting net likelihood for severe shaking (~0.9 g peak ground acceleration) in Tokyo, Kawasaki, and Yokohama for the next 30 years is ~30%. The long historical record in Kanto also affords a rare opportunity to calculate the probability of shaking in an alternative manner exclusively from intensity observations. This approach permits robust estimates for the spatial distribution of expected shaking, even for sites with few observations. The resulting probability of severe shaking is ~35% in Tokyo, Kawasaki, and Yokohama, and ~10% in Chiba for an average 30-yr period, in good agreement with our independent estimate, and thus bolstering our view that Tokyo's hazard looms large. Given $1 trillion estimates for the cost of an M~7.3 shock beneath Tokyo, our probability implies a $13 billion annual probable loss.

1. Introduction

The Japanese government recently issued a report furnishing a probabilistic hazard assessment for large earthquakes on the plate boundary megathrusts and the 98 most active faults in Japan and their associated shaking [*Earthquake Research Committee*, 2005]. Our Japan-US team sought to probe more deeply into the areas of greatest uncertainty identified by the government study, developing new data sets and analytical methods, and pursuing new means to corroborate our derived probabilities. We relied on observational evidence rather than models of seismic behavior wherever possible, focusing greatest attention on the likelihood of earthquakes capable of producing severe shaking (Japan Meteorological Agency JMA Intensity 6, equivalent to a peak ground acceleration of ~0.9 *g* [*Karim and Yamazaki*, 2002]) in the highly populated Tokyo-Yokohama corridor and the southern Kanto plain. Here we summarize our broad approach and conclusions.

2. Kanto plate tectonic configuration

Three of the Earth's tectonic plates meet 300 km east of Tokyo, and a chain of active volcanoes lies just 100 km to the west (Figure 1a). To understand the geometry of this so-called 'triple junction' and to identify the faults on which large earthquakes can strike, we examined 320,000 microearthquakes in a 3D geographic information system and used 6,000 of these to carry out a seismic tomographic inversion [*Toda et al.*, 2006]. On the basis of the microearthquake distributions, seismic tomography, and seismic stress inversion, we propose that a 90 x 120-km-wide dislodged fragment of the Pacific plate is wedged beneath Tokyo between the Pacific, Philippine Sea and Eurasian plates (Figure 1b). The fragment was probably dislodged when two seamount chains collided at the Japan Trench about 2 million years ago. We suggest that the fragment controls much of Tokyo's seismic behavior, with the concentration of M≤7.4 shocks beneath Tokyo attributable to the sliding of the fragment against the three other plates. Unlike previous interpretations, in which the Philippine Sea plate was thought to extend 100 km north of Tokyo and reach to a depth of 90 km [*Ishida*, 1992; *Noguchi*, 1998], we argue that the Philippine Sea slab extends to a depth of only 35 km. If so, the leading edge of the Philippine Sea slab, and thus the northward limit of great underthrust earthquakes, extends only as far north as Tokyo (Figure 1b). This interpretation differs from the prevailing view, in which all of the seismicity beneath Tokyo is attributed to the

Philippine Sea plate warped and folded against the Pacific plate [*Ishida*, 1992, 1995]. The analogous bend in the Japan trench between the Japanese islands of Honshu and Hokkaido also is associated with the collision of a seamount chain, leading to a severely bent Pacific plate slab [*Niu et al.*, 2005] and concentrated inland seismicity beneath the Hidaka basin. Unlike Kanto basin, the Hidaka basin is not associated with a triple junction, and so we regard the seismic features of the Kanto region to be principally related to the Pacific Plate, rather than to the Philippine Sea plate.

3. Historical earthquake intensities

Compilations of earthquake shaking during 1600-1884 [*Usami*, 1994; *Usami*, 2003], 1884-1923 [*Utsu*, 1979, 1982] and 1923 [*Takemura*, 2003] [*Hamada et al.*, 2001], were combined with post-1923 data through 2003 [*Japan Meteorological Agency*, 2004], to produce a new digital database of 10,000 intensity observations for the Kanto region [*Bozkurt et al.*, 2006]. Intensity is generally based on written observations of shaking (Table 1), and so can be used to assess earthquakes that precede the development of seismic instrumentation. The peak intensity observed within 2000 5 x 5 km cells during the past 400 years is shown in Figure 2a. For cells containing observations for the three largest earthquakes to occur in the Kanto region during this period, similar and severe (JMA Intensity ≥6) shaking intensity is seen (Figure 2b-d). These observations indicate that the 1703, 1855, and 1923 earthquakes were large, and also indicate that unconsolidated stream deposits in the Kanto plain and young sediments along the western margin of Tokyo Bay amplify the shaking.

4. Size, geometry, and location of the three largest earthquakes

1 September 1923 Kanto earthquake

To evaluate the release of accumulated plate motion in the Kanto region, we reassessed the 1923 earthquake fault geometry and slip [*Nyst et al.*, 2006b]. The model provides a best fit to a new geodetic dataset consisting of vertical displacements from leveling and angle changes from triangulation measurements obtained in surveys between 1883 and 1927. We used ten times more triangulation data than were previously available, and also corrected the observations to remove interseismic deformation (the steady deformation that occurs during the centuries between earthquakes, that is roughly opposite in sign to the coseismic motions). The location, depth, and dip of the fault

planes is adopted from a recent seismic reflection study of the Kanto region [*Sato et al.*, 2005]. The fault model consists of two adjacent 20°-dipping low-angle planes accommodating oblique reverse right-lateral slip of 6.0 m on the larger eastern plane and 9.5 m on the smaller western plane [*Nyst et al.*, 2006b] (Figure 3a). Two sites of high slip are identified, one at the west end of the fault near the epicenter, the other beneath the mouth of Tokyo Bay [*Pollitz et al.*, 2005; *Pollitz et al.*, 2006]. Most of aftershocks of the 1923 earthquake occurred in regions where we calculate that stress transferred by the earthquake brought nearby faults closer to failure (red zones *1-2* in Figure 3a).

11 November 1855 M~7.3 Ansei-Edo earthquake

On the basis of intensity observations and reported aftershock activity, *Bakun* [2005] estimated M=7.2 ($6.9 \leq M \leq 7.5$ at 95% confidence), an epicenter at the north margin of Tokyo Bay, and a depth between 30-70 km. By excluding less reliable JMA Intensity 3 (felt) observations, *Grunewald* [2006] concluded that the event was M=7.4, with an epicenter near Chiba (Figure 2c and Figure 4a). A nearly identical distribution of intensities was observed for the 23 July 2005 M=6.0 earthquake at 70 km depth beneath Chiba, suggesting that the Ansei-Edo event might also lie at the same depth, corresponding to the North Tokyo Bay seismic cluster at the contact between the proposed Kanto fragment and the Pacific Plate [*Toda et al.*, 2006] (Figure 3b and Figure 1). The northern Tokyo Bay and southern Kanto Plain have been the site of four $M \geq 7$ shocks since 1649 (Figure 4a), although no such earthquakes have struck since 1923. This seismic hiatus may have occurred because stress on the fault that ruptured in 1855 was subjected to a stress decrease by the 1923 Kanto earthquake [*Nyst et al.*, 2006a], inhibiting failure (Figure 3a).

31 December 1703 M~8.2 Genroku earthquake

Using earthquake intensity data (Figure 2d), shorelines uplifted and deformed by the 1703 earthquake [*Shishikura*, 2003], a newly augmented tsunami run-up height dataset, and intensity data [*Grunewald*, 2006], we propose that the 1703 earthquake ruptured the Sagami trough fault segment at the mouth of Tokyo Bay (Fault A in Figure 5a), plus one or two segments located east of the Boso peninsula (Faults B and C in Figure 5a), resulting in a magnitude of M~8.2 [*Shishikura et al.*, 2006]. Slip of the same amount also occurred in 1923 (Figure 3a). Slip on Fault B is needed to explain why the uplift of the eastern Boso peninsula was much greater in 1703 than in 1923, and Fault C is needed to

explain why the 1703 shock was accompanied by a substantial tsunami on the eastern Boso peninsula shore (Figure 5a). Because the fault trace undergoes a 40° bend near the tip of the Boso peninsula, the earthquake uplift is not recovered as a result of interseismic deformation (the relaxation of the lower crust) or slip on adjacent fault segments, and so a set of uplifted marine terraces preserves the prehistoric record of great earthquakes along the eastern Sagami trough (Figure 5b). Greater Tokyo experienced a century of seismic quiescence after the 1703 earthquake [*Okada*, 1994], and by analogy to the 1923 earthquake most faults north of Fault A would have been inhibited from failure by the stress transferred by the 1703 event (Figure 3a).

5. Historical earthquake magnitudes and locations

Following *Bakun and Wentworth* , we use observed intensity distributions to estimate the magnitude, location, and approximate depth of historical earthquakes, as well as the covariance between location and magnitude. A set of 25 earthquakes with both intensity data and instrumental magnitudes, locations, and depths were used to develop a calibrated intensity attenuation relation (in other words, how shaking decays with earthquake size and with distance from the epicenter) for the Japanese archipelago [*Bakun*, 2005]. This relation was applied by *Grunewald* [2006] to relocate earthquakes during the period 1600-1884 (Figure 4). Some 15 shocks had sufficient intensity observations for stable solutions; analysis suggests that all M≥6.75 shocks should be contained in our catalog (Figure 6a and Appendix Figure 1).

6. Associating earthquakes with faults

The distribution and magnitude of deformation observed by GPS and geodetic leveling enabled *Nishimura and Sagiya* [2006] to estimate the strain accumulation rate on the major faults, and thus to infer their seismic slip rates. The tectonic model introduced in Figure 1 [*Toda et al.*, 2006] supplied the fault locations and geometry. This analysis reveals that along the Suruga and Sagami troughs (sites of the 1854 M=8.4 Tokai, 1923 M=7.9 Kanto, and 1703 M~8.2 Genroku earthquakes), faults are locked and are thus accumulating strain to be released in future earthquakes (Figure 7). In contrast, north of the Izu peninsula, the plate boundary faults partially creep and so produce earthquakes less frequently. Along the Japan Trench, the site of the 1938 M~7.5 earthquake swarm are locked, but the remainder of the Pacific subduction zone is creeping and thus

apparently has a low seismic potential. Overall, the inferred seismic slip rate is highest for the 1938 fault, intermediate for the faults on which the 1703, 1854, and 1923 earthquakes struck, and is poorly resolved for the presumed 1855 earthquake fault (Figure 7).

The slip sustained in an earthquake, when divided by the fault slip rate, should correspond to the time between earthquakes (the inter-event time). Given the 6 m of oblique (right-lateral reverse) slip in the 1923 Kanto and 1703 Genroku earthquakes, and the inferred ~25 mm/yr mean slip rate (Figure 7), the mean inter-event time should be ~250 yr, considerably less than the ~403±66 yr (95% confidence) inter-event time observed from the marine terrace record (Figure 5b). This disparity could mean that episodic or aseismic slip occurs on the fault that ruptured in 1923 and 1703, although GPS observations of such creep events are restricted to an area east of the Boso peninsula [*Sagiya*, 2004].

7. The balance of seismic strain energy accumulation and release

Over a sufficiently long period, the rate of strain energy (or seismic moment) accumulation manifest in crustal deformation must balance the rate of seismic strain released in earthquakes. *Nishimura and Sagiya* [2006] estimated the rate of seismic moment accumulation by the product of the fault areas and their slip rates from Figure 7, multiplied by an assumed crustal stiffness (or elastic modulus). The earthquakes in the historical catalog are represented by probability density functions for location and magnitude (Appendix Figure 1). Through Monte Carlo simulation, *Grunewald* [2006] estimated the most probable seismic moment release rate for A.D. 1649-2005 in the greater Kanto region from the catalog. From this estimate, it is evident that the energy accumulation measured geodetically likely balances energy release represented by the earthquake catalog, indicating that the catalog is long enough to capture the range of seismic behavior (Figure 8). From this balance we further infer that there is currently neither an earthquake deficit nor an earthquake overabundance. This balance neglects permanent deformation, but since the Quaternary coastal uplift is hundreds of meters and the cumulative fault slip is tens of kilometers, its influence is small and most energy is elastic.

8. Prehistoric record of great earthquakes

The Boso peninsula shoreline contains 16 marine terraces, each uplifted about 1.0-1.5 m during the past 7,000 years and dated by *Shishikura* [2003] (Figure 5b). The southern tip of the Boso peninsula was uplifted 6.0 m in 1703 and 1.8 m in 1923. Although the 1703 Genroku shock was much larger than the 1923 Taisho earthquake, the inferred slip on the fault segment at the mouth of Tokyo bay is similar, about 6-8 m (Fault A in Figure 5a); the 1703 earthquake also rupturing one or more segments to the east, resulting in greater Boso peninsula uplift. This suggests that each great Sagami trough earthquake permanently uplifts a marine terrace. Four of the southern Boso terraces were uplifted 4-6 m, and these resemble deformation that accompanied the 1703 M~8.2 Genroku earthquake (Figure 5a). Thus, by treating all terrace uplift events in a single a time series, we are measuring the recurrence behavior of the Tokyo bay Fault A, which slipped in all of the M≥7.9 shocks.

9. Probability for M≥7.9 Kanto earthquakes

Large earthquake recurrence on a single fault is thought to be cyclic, and so the probability of the next earthquake depends on the time since the last one. When considering many faults in a region, the time-dependence of stress renewal on each individual fault is averaged out, and so a time-independent or Poisson probability may become appropriate. A Poisson probability can be regarded as a time-averaged estimate, rather than one in which the underlying process is random. In seismic hazard investigations, a further reason to employ a Poisson probability is that fewer assumptions are needed, and each assumption carries additional uncertainty. For the time-averaged probability (the likelihood of an earthquake during an *average* 30-yr period), we require only the mean inter-event time and its uncertainty or aperiodicity for earthquakes of interest, such as the M~8 'Taisho' events on the Sagami fault. (Aperiodicity is 0 for perfectly regular recurrence, and 1 for perfectly random occurrence.) For time-dependent probabilities (the likelihood during the *next* 30 years), we use the time that has elapsed since, for example, the 1923 Taisho-type earthquake, and assume a probability density function to describe how the hazard grows with time since 1923. Required for both probability estimates are the dates of past events and the assumption that the fault slips approximately the same amount in each earthquake; the greater the number of dated earthquakes in the time series, the more useful the series

becomes. Over many earthquake cycles, the Poisson probability will be the average of the renewal probabilities.

To estimate the Poisson probability of Taisho (1923 M≥7.9 type) earthquakes, we plot the frequency of all shocks within the Kanto area as a function of magnitude in Figure 6a. This region includes the Sagami trough but excludes the Suruga trough, because the M~8 Tokai earthquakes there in 1707 and 1854 (Figure 1) did not cause JMA Intensity 6 shaking in Tokyo. We combine modern instrumental, historical, and paleoseismic data into one plot, which is fit by a Gutenberg-Richter relation for 4.5<M≤8.2. Whether the function is truncated depends on if the largest earthquakes are undersampled; both interpretations (the solid and dashed lines in Figure 6a and 6b) are viable. Converting frequency, λ, into probability, P, by the relation $P = 1–(\exp- \lambda N)$, where N is the time period (here, 30 yr), we derive Figure 6b. Thus, for Taisho type (M≥7.9) earthquakes, the probability is 8-11% (Figure 6b).

For the renewal probability we use a new method, detailed in the Appendix, to find the likely interevent time and periodicity for 1923-type ('Taisho') events (Figure 9). Remarkably, the resulting Taisho earthquake occurrence is more regular than for earthquakes of the same size and frequency on the San Andreas fault, where the aperiodicity is ~0.8 [*Parsons*, 2005; *Weldon et al.*, 2005; *Weldon et al.*, 2004]. Our renewal probability is more tightly constrained and slightly lower than that of the Japanese government; it is also well below the Poisson estimate because we are currently only 20% into the mean earthquake cycle for M≥7.9 Taisho shocks (Figure 9c).

10. Probability for M≥7.1 Ansei-Edo type earthquakes

Considering location and magnitude uncertainties, there have been six to seven M≥7 shocks within 50 km of Tokyo since 1649. Among the largest is the 1855 Ansei-Edo event, which produced JMA Intensity 6 shaking over much of the southern Kanto Plain (Figure 2c). The Kanto seismic corridor [*Toda et al.*, 2006] currently contains the highest rate of Kanto seismicity (Figure 3b), as well as most of the moderate historical earthquakes (Figure 4a). Thus, we plot the frequency of all earthquakes within this corridor as a function of magnitude in Figure 6c, which is well fit by a Gutenberg-Richter relation. We have no paleoseismic record for Ansei-Edo events, since they are deep and leave little morphological evidence of their occurrence. We judge that most M≥7.1 shocks that fall within the corridor can produce JMA Intensity 6 shaking in

Tokyo. The resulting probability is shown in Figure 6d, yielding ~20% in 30 years, although the confidence range in the historical catalog is quite wide. The uncertainty would be much smaller if 4.0≥M≥7.5 earthquake rates were fit in Figure 6b. Details of this calculation are presented in the Appendix.

Deducing a renewal probability for Ansei-Edo type events is hampered by several sources of uncertainty, but it is likely quite high. If, on the basis of their very similar intensity distributions, one assumes that the 1855 earthquake occurred at the location and 70 km depth of the 23 Jul 2005 earthquake [*Grunewald*, 2006], then the 1855 earthquake resulted from thrust slip between the base of the Kanto fragment and the underlying Pacific plate. Velocity reconstructions by *Toda et al* [2006] give a slip rate of ~55 mm/yr on this surface for the past 2 Ma. Based on the 7.2≤M≤7.5 size of the 1855 earthquake and magnitude-slip scaling relationships from *Wells and Coppersmith* [1994], the mean slip would have been ~3-8 m. This would yield a 50-150 yr inter-event time. Even though the aperiodicity of this cycle cannot be assessed, we are now at or beyond the end of an earthquake cycle. Thus, the renewal probability would be much greater than the Poisson probability. A counter-argument is that only one earthquake of this size is evident in the 400-year historical record in the Kanto seismic corridor, so the interevent time should be higher than our estimate. If the 1703 and 1923 shocks each inhibited the occurrence of Ansei-Edo shocks for 50-100 years (Figure 3a), however, the historical record would be too short to be representative.

11. Combined earthquake probabilities

The combined time-averaged or Poisson 30-yr probability for intensity≥6 shaking is thus 29%, although the 67% confidence range on this estimate is wide (7-40%) because of the limitations of the historical catalog. For the renewal probability, the likelihood of Ansei-Edo earthquakes is ≥35%, and for Taisho (1923-type) earthquakes it is <1%, and so we can only suggest that the combined renewal probability is likely to be much higher than 35% (Table 2). These probabilities correspond to the occurrence of JMA Intensity 6 shaking in greater Tokyo. *Karim and Yamazaki* [2002] used a set of earthquakes with intensity observations and strong ground motion data to deduce the ground acceleration and velocity values associated with the intensities (Table 1), finding that JMA Intensity 6 corresponds to a peak horizontal ground acceleration (PGA) of 0.95 g (0.7-1.5 g) and a peak ground velocity (PGV) of 0.93 m/s (0.5-1.0 m/s). Because intensities were

historically measured in 1-2 story wood or masonry buildings, they are principally sensitive to accelerations in the 5-8 Hz frequency range.

12. Model corroboration by observed intensities

To corroborate our probability models, we constructed a time-averaged assessment exclusively from the observed intensities [*Bozkurt et al.*, 2006]. This method assumes only that the 400-year catalog is representative of the long-term seismic behavior, an assumption consistent with the balance between catalog strain energy release and geodetically estimated energy accumulation (Figure 8). For this assessment we neither locate nor estimate the size of earthquakes, nor do we identify fault sources or their slip rates. Instead, we simply plot the frequency-intensity distribution for all 10,000 intensity observations, and fit the decay to an exponential relation (Figure 10a). A power law satisfies the data nearly as well. The same exponent is then fit to the small number of observations that are typically available in each of 2000 5 x 5 km cells throughout Kanto (Figure 10b-c), to produce a spatially variable probability map. The resulting probabilities (Figure 11a) reveal a positive correlation with proximity to the major plate boundary faults, as well as with stream deposits and bay mud that amplify the shaking in unconsolidated sediments (Figure 11b). The resulting probability of experiencing intensity≥6 shaking is 37% in Tokyo, 34% in Yokohama, and 11% in Chiba, in good agreement with our other estimate (Table 2).

13. Human, structural, and financial and consequences of a large Tokyo earthquake

The Cabinet Office of the Japanese government recently issued a risk assessment for large Tokyo earthquakes [*Central Disaster Management Council*, 2005]. They considered an M=7.3 earthquake beneath Tokyo, similar to the 1855 Ansei-Edo shock. The 240,000-840,000 destroyed buildings in their estimate depends strongly on wind speed and time of day, because high winds spread fire and rush hour exposes people to falling objects. If a M=7.3 earthquake struck at 6 PM in 15 m/s (33 mph) winds, the Cabinet office estimates 11,000 deaths, 210,000 wounded, and 96 million tons of wreckage. About 57% of the deaths and 77% of the housing collapses are attributable to fire, and 28% of deaths and 18% of the collapses are due to shaking. The projected cost of a M=7.3 earthquake beneath Tokyo are $1.0 trillion (USD), which is 130% of the Japanese annual budget [*Central Disaster Management Council*, 2005]. Only about 5% of this loss is thought to be insured, and so the cost would be borne principally by home and business owners and

the government. The total is comprised of $587 million direct losses associated with recovery and rebuilding, and $395 million in indirect losses due to production declines within and outside of Tokyo.

Our 29% probability of an M~7.3 Tokyo earthquake in 30 years corresponds to an annual probability of 1.2%. Thus, the annual probable loss for Tokyo is $12 billion. Thus, in order to pay for the future earthquake, the Japanese government would need to save this amount annually, investing a portion to mitigate against future losses. But irrespective of Japanese actions, the consequences of a Tokyo earthquake of this magnitude are unlikely to be restricted to Japan. Japan is the largest owner of U.S. Treasury securities, holding $700 billion or 17% of the total. How global capital markets would respond to a sudden withdrawal of these and other funds is unknown.

14. Conclusions

We have pursued several approaches to estimating the likelihood of severe earthquake shaking in greater Tokyo. The time-averaged and renewal earthquake probabilities both tend to produce answers of about 30% likelihood of intensity≥6 shaking in the next 30 years. The weakness in our renewal probability is uncertainty on the inter-event time for 1855 Ansei-Edo type events; the weakness in our Poisson probability is that it may not reflect conditions that govern earthquake occurrence for the next 30 years. But the singular benefit of the Poisson probability is that it can be corroborated by the observed intensity data free of most modeling assumptions. Such confirmation is rare if not unprecedented in seismic hazard analysis, and so in our judgment makes our findings credible, and the consequences sobering.

Acknowledgements. We are grateful for reviews by Willy Aspinall, George Helffrich, Steve Sparks, and William Bakun. We appreciate principal funding by Swiss Re, as well as for contributions by the National Institute of Advanced Industrial Science and Technology (AIST) of Japan, and the U.S. Geological Survey. We also thank the members of Team Tokyo, whose work this paper synthesizes: William Bakun, Martin Bertogg, Serkan Bozkurt, Atsushiro Dodo, Elliot Grunewald, Mariagiovanna Guatteri, Nobuo Hamada, Ryoichi Nakamura, Takuya Nishimura, Marleen Nyst, Yoshimitsu Okada, Tom Parsons, Fred Pollitz, Takeshi Sagiya, Kenji Satake, Masanobu Shishikura, Wayne Thatcher, and Silvio Tschudi. Team Tokyo publications, presentations, computer animations, GIS imagery, and earthquake event sets can be downloaded from our web site,

http://sicarius.wr.usgs.gov/tokyo/

15. Appendix

Time-Dependent Probability. The renewal probability P is calculated by integrating a probability density function $f(t)$

$$P(t \le T \le t + \Delta t) = \int_t^{t+\Delta t} f(t)dt \qquad (1)$$

between t and $t + \Delta t$, where $f(t)$ can be any appropriate distribution with the property that probability grows with time after the last event. We use a Brownian Passage Time distribution [*Matthews et al.*, 2002] to describe how the hazard grows with time

$$f(t,\mu,\alpha) = \sqrt{\frac{\mu}{2\pi\alpha^2 t^3}} \exp\left(-\frac{(t-\mu)^2}{2\mu\alpha^2 t}\right) \qquad (2)$$

where μ is the mean interevent time, and α is the aperiodicity of the distribution, which grows with inherent recurrence variability. Lognormal or Weibull distributions would yield similar results for periods starting in 2005.

We seek to find all recurrence and variability behavior that can satisfy observations with a Brownian Passage Time distribution. Using a newly developed method [*Parsons*, 2005] and the marine terrace record (Figure 5b and Table 3), we constructed Brownian Passage Time distributions for all combinations of interevent times from 250-750 yr and aperiodicities from 0.1-0.9. For every pair of trial interevent times and aperiodicities, we randomly drew a sequence of interevent times in 5 million trials, starting with the oldest event, retaining the sequence only if all ~17 events fell within the observed earthquake age ranges in Table 3. The vast majority of such draws do not match the observations, but the distribution of the 2150 successful matches is contoured in Figure 9a. The majority of the distributions fell within a narrow range: a mean interevent time of 403±66 years (95% confidence), with a mean 0.28 aperiodicity (0.2-0.4 at 92% confidence). The resulting 30-yr probabilities for the likelihood of a M≥7.9 earthquake on the Sagami trough (Fault A in Figure 5) during the 30 yr period, 2006-2035, range from 0% to 6%, with the dominant peak between 0-0.5% in 2005 (Figure 9b).

Earthquake magnitude-frequency relation. We seek to assess the time-averaged (Poisson) likelihood of JMA Intensity 6 shaking in greater Tokyo. We thus plot the frequency of earthquakes as a function of magnitude for the Kanto region, which includes the Sagami but excludes the Sagami trough (Figure 6a). We combine M≥1.5 earthquakes recorded since 1997, M≥4.5 earthquakes since 1924, M≥6.7 earthquakes since 1649, and M≥7.9 earthquakes since 7500 years before present (from the marine terrace record) in one continuous curve in Figure 6b. The 0.96 slope of the magnitude-frequency curve (called a 'b-value') is typical of tectonic seismicity (where 0.9≥b≥1.1), and the resulting frequency of M≥7.9 shocks can be transformed into a probability for a 30-yr period of 9-11% (Figure 6c) using $P = 1 - \exp(-\text{rate} \times \text{period})$.

Smaller earthquakes within the highly active Kanto seismic corridor (Figure 3b), such as the 1855 Ansei Edo shock, also produced JMA Intensity 6 shaking in Tokyo and Yokohama, so we plot a separate frequency-magnitude curve for this subset of the Kanto region. Whether a given earthquake falls within this smaller box is highly dependent on the location uncertainty. So, rather than use the intensity center locations and their associated magnitudes shown in Figure 4a, we created 1000 realizations of the catalog by Monte Carlo simulation, drawing the earthquake locations according to the probability density functions. For example, it is evident in Appendix Figure 1 that in ~50% of the samples, the 1855 earthquake would fall within the Kanto seismic corridor, and in only 5% of the sampling would the 1856 earthquake lie within the corridor. Each earthquake location specifies a magnitude, and we further assume that the magnitude contours are uncertain by ±0.1 magnitude units. We plot the mean and ±1-sigma bounds on the frequency-magnitude relation for the 1000 realizations of the catalog to capture the uncertainty inherent in the historical catalog locations and their covariance with magnitude. The resulting frequency curve is shown in Figure 6c and the 30-yr probability is shown in Figure 6d. When these two probabilities are combined, the net probability for JMA Intensity 6 shaking in the greater Tokyo area is 29% (Table 2).

16. Audience questions from the 26 October 2005 *Stein et al*. presentation at the Royal Society Discussion Meeting on Extreme Natural Hazards

Q. Prof. Russell Blong, Benfield Australia: *What is the relationship between the 1703 Genroku earthquake and the 1707 Fuji eruption? If it was not fortuitous, why wasn't there an eruption after the 1923 earthquake? Will there be an eruption after the next great earthquake*?

A. These are fascinating questions that we hope to probe in a subsequent study.

The 31 December 1703 M~8.2 Genroku shock struck along the Sagami trough. Its western end lies just 40 km east of Mt. Fuji. On 4-7 February 1704, sounds emanated from Mt. Fuji that volcanologists today believe might indicate magma migration. Then, on 28 October 1707, the M~8.6 Tokai shock struck along the Suruga trough. Both great earthquakes occurred on the Philippine Sea plate slab. The nearest edges of the two great rupture surfaces were only about 80 km apart, and Mt. Fuji lies between them. Some 49 days after the Tokai earthquake, the Hoei eruption of Mt. Fuji began, one of the most violent in Fuji's 10,000-year history, with a tephra volume of 3 km^3 and a volcanic explosivity index of 5. This was the largest of the 30 or so eruptions of Fuji since 930 BC. There are reported to be frequent swarms of earthquakes beneath Fuji during the period between the Tokai earthquake and the Hoei eruption, although at least some of these are probably Tokai aftershocks. The 1923 Kanto earthquake caused no eruption of any kind, although some 1923 aftershocks also occurred at or near Mt. Fuji [*Nat. Mus. Japanese History*, 2003].

We would like to study the earthquake and eruption time series more closely to see if they are correlated. Because great Tokai shocks recur roughly every 200 years and great Kanto shocks recur roughly every 400 years, few of these earthquakes can have triggered more than minor eruptive activity. We would also like to test whether Coulomb stresses imparted by the 1703 earthquakes might have compressed the magma chamber or opened magma conduits beneath Fuji, whether the 1703 shock promoted failure on the Suruga megathrust, and whether the Tokai earthquake, in turn, further compressed the magma chamber, triggering or hastening the eruption. We hypothesized such an interaction between the 1990 M=7.8 Luzon earthquake and the Mt. Pinatubo eruption 6 months later [*Bautista et al.*, 1996], and for the history of Apennine earthquakes and Vesuvius eruptions [*Nostro et al.*, 1998].

Q. Prof. Stephen Sparks, Bristol University: *How are the Japanese authorities responding to scientific information, and to the high probability of a Tokyo earthquake*?

A. This remains to be seen, but earthquakes are felt in Tokyo about once every two weeks, and these are probably the strongest public reminder of the looming risk. The Japanese government released its first-ever probabilistic earthquake hazard assessment in 2004, a departure from a historical focus on earthquake prediction. We regularly briefed the head of the Government committee and members of his scientific team as we developed our findings, and they have generally been welcoming and receptive. Nevertheless, we have not approached any governmental authorities because we did not want to appear to be challenging the government committee. The Royal Society discussion meeting was the first public presentation of our results, and we have yet to present a similar summary to the Japanese public.

Q. Prof. Haresh Shah, RMS and Stanford University: *Since an insurance company supports your work, do you have plans to extend your work from seismic hazard to seismic risk for the Tokyo region*?

A. Although we do not calculate the probability of the human or financial losses associated with a particular earthquake, we have added a brief discussion of the earthquake consequences based on Japanese research. We have also placed on our Team Tokyo web site an event set of the intensity distributions for the 15 largest earthquakes that have struck the greater Tokyo region during the past 400 years. Insurance companies and risk consulting companies can use these as scenario events to calculate losses to their insurance portfolios, building and lifeline inventories, or casualties.

Q. Mr. James Kennedy, public attendee: *What is the distinction between earthquake prediction and forecasting*?

A. Among earthquake researchers, 'prediction' is taken to mean an earthquake time, place, and magnitude, with a high degree of specificity and reliability. This has not been achieved. A 'forecast' supplies the probability of these parameters over a given time period. The USGS issues reports containing 30-year forecasts, and has a web site that issues 24-hour forecasts, http://pasadena.wr.usgs.gov/step/

16. References

Bakun, W. H. (2005), Magnitude and location of historical earthquakes in Japan and implications for the 1855 Ansei Edo earthquake, *J. Geophys. Res.*, *110*, doi:10.1029/2004JB003329.

Bakun, W. H., and C. M. Wentworth (1997), Estimating earthquake location and magnitude from seismic intensity data, *Bull. Seismol. Soc. Amer.*, *87*, 1502-1521.

Bautista, B. C. et al. (1996), Relationship of regional and local structures to Mount Pinatubo activity, in *Fire and Mud: Eruptions and Lahars of Mount Pinatubo, Philippines*, edited by R. S. Punongbayan and C. G. Newhall, pp. 351-370, Philipp. Inst. Volc. Seismol., Qezon City—Univ. Washington Press, Seattle, Seattle.

Bozkurt, S., R. S. Stein, and S. Toda (2006), Forecasting probabilistic seismic shaking for greater Tokyo based on 400 years of intensity observations, *in prep*.

Central Disaster Management Council (2005), Report of the 15th special committee on the earthquake just beneath the Tokyo metropolis, 25 Feb., Cabinet Office, Gov. of Japan, Tokyo.

Earthquake Research Committee (2005), Comprehensive study of probabilisitic seismic hazard map for Japan, 125 pp, Headquarters for Earthquake Research Promotion, Tokyo.

Fujiwara, O., and T. Kamataki (2003), Significance of sedimentological time-averaging for estimation of depositional age by ^{14}C dating on molluscan shells, *Quaternary Res. (Japan)*, *42*.

Fujiwara, O., F. Masuda, T. Sakai, T. Irizuki, and K. Fuse (1999), Holocene tsunami deposits detected by drilling in drowned valley of the Boso and Miura Peninsulas, *Quaternary Res. (Japan)*, *38*, 41-58.

Grunewald, E. (2006), A new historical catalog of destructive earthquakes near Tokyo and implications for the long-term seismic process, *J. Geophys. Res.*, *submitted*.

Hamada, N., Y. Kazumitsu, M. Nishwaki, and M. Abe (2001), A comprehensive study of aftershocks of the 1923 Kanto earthquake, *Bull. Seism. Soc. Japan*, *54*, 251-265.

Ishida, M. (1992), Geometry and relative motion of the Philippine Sea plate and Pacific plate beneath the Kanto-Tokai district, Japan, *J. Geophys. Res.*, *97*, 489-513.

Ishida, M. (1995), The seismically quiescent boundary between the Philippine Sea plate and the Eurasian plate in central Japan, *Tectonophysics*, *243*, 241-253.

Japan Meteorological Agency (2004), Annual Seismological Bulletin (CD-ROM), edited, JMA, Tokyo.

Karim, K. R., and F. Yamazaki (2002), Correlation of JMA instrumental seismic intensity with strong motion parameters, *Earthquake Engng. Struct. Dyn.*, *31*, 1191-1212, doi: 1110.1002/eqe.1158.

Matthews, M. V., W. L. Ellsworth, and P. A. Reasenberg (2002), A Brownian model for recurrent earthquakes, *Bull. Seismol. Soc. Amer.*, *92*, 2233– 2250.

Nakata, T. et al. (1980), Holocene marine terraces and seismic crustal movements in the southern part of Boso Peninsula, Kanto, Japan, *Geograph. Rev. Japan, Ser. A*, *53*, 29-44.

Nat. Mus. Japanese History (2003), *Documenting Disaster: Natural disasters in Japanese history, 1703-2003*, 167 pp., Foundation for Museums of Japanese History, Chiba.

Nishimura, T., and T. Sagiya (2006), Crustal block kinematics around the northernmost Philippine Sea plate, central Japan estimated from GPS and leveling data, *J. Geophys. Res.*, *submitted*.

Niu, F., A. Levander, S. Ham, and M. Obayashi (2005), Mapping the subducting Pacific slab beneath southwest Japan with Hi-net receiver functions, *Earth Planet. Sci. Lett.*, *239*, 9-17, doi:10.1016/j.epsl.2005.1008.1009.

Noguchi, S. I. (1998), Seismicity, focal mechanisms and location of volcanic front associated with the subducting Philippine Sea and Pacific plates beneath the Kanto district, Japan, *Bull. Earthq. Res. Inst. Univ. Tokyo*, *73*, 73-103.

Nostro, C., R. S. Stein, M. Cocco, M. E. Belardinelli, and W. Marzocchi (1998), Two-way coupling between Vesuvius eruptions and southern Apennine earthquakes (Italy) by elastic stress transfer, *J. Geophys. Res.*, *103*, 24,487-424,504.

Nyst, M., N. Hamada, F. F. Pollitz, and W. Thatcher (2006a), The stress triggering role of the 1923 Kanto earthquake, *J. Geophys. Res.*, *submitted*.

Nyst, M., T. Nishimura, F. F. Pollitz, and W. Thatcher (2006b), The 1923 Kanto earthquake re-evaluated using a newly augmented geodetic data set, *J. Geophys. Res.*, *in press*.

Okada, Y. (1994), Seismotectonics in the Tokyo metropolitan area, central Japan, *Proceedings of the 9th joint meeting of the U.J.N.R. Panel on Earthquake Prediction Technology*, *9*, 47-59.

Parsons, T. (2005), Signifcance of stress transfer in time-dependent earthquake probability calculations, *J. Geophs. Res.*, *110*, doi: 10.1029/2004JB003190.

Pollitz, F., M. Nyst, and T. Nishimura (2005), Coseismic slip distribution of the 1923 Kanto earthquake, Japan, *J. Geophys. Res.*, *110*, B11408, doi: 11410.11029/12005JB003638.

Pollitz, F., N. Nyst, T. Nishimura, and W. Thatcher (2006), Inference of postseismic deformation mechanisms following the 1923 Kanto earthquake, *J. Geophy. Res.*, *in press*.

Sagiya, T. (2004), Interplate coupling in the Kanto district, central Japan, and the Boso silent earthquake in May 1996, *Pure and Applied Geophys.*, *161*, 2601-2616.

Sato, H. et al. (2005), Earthquake source fault beneath Tokyo, *Science*, *309*, *10.1126/science.1110489*, 462-464.

Shishikura, M. (2003), Cycle of interplate earthquakes along the Sagami Trough deduced from tectonic geomorphology, *Bull. Earthq. Res. Inst. Univ. Tokyo*, *78*, 245-254.

Shishikura, M., S. Toda, and K. Satake (2006), Fault model of the 1703 Genoku Kanto earthquake (M 8.2) along the Sagami trough deduced from renewed coseismic crustal deformation, *in prep.*

Takemura, M. (2003), *The Great Kanto Earthquake, Knowing Ground Shaking in Greater Tokyo Area (in Japanese)*, 139 pp., *Kajima Institute Publishing*, Tokyo.

Toda, S. et al. (2006), A slab fragment wedged beneath Tokyo: Consequences for earthquakes, volcanoes and geography, *Nature*, submitted.

Usami, T. (1994), *Seismic intensity maps and isoseismal maps of historical earthquakes of Japan*, Japan Electric Association, Tokyo.

Usami, T. (2003), *Materials for comprehensive list of destructive earthquakes in Japan [416]-2001*, 607 pp., Univ. Tokyo Press, Tokyo.

Utsu, T. (1979), Seismicity of Japan from 1885 through 1925 – a new catalog of earthquakes of M≥6 felt in Japan and smaller earthquakes which caused damage in Japan, *Bull. Earthq. Res. Inst. Univ. Tokyo*, 253-308.

Utsu, T. (1982), Catalog of large earthquakes in the region of Japan from 1885 through 1980, *Bull. Earthq. Res. Inst. Univ. Tokyo*, *57*, 401-463.

Weldon, R. J., T. E. Fumal, G. P. Biasi, and K. M. Scharer (2005), Past and Future Earthquakes on the San Andreas Fault, *Science*, *308*, 966-967.

Weldon, R. J., K. M. Scharer, T. E. Funaml, and G. P. Biasi (2004), Wrightwood and the earthquake cycle: What a long recurrence record tells us about how faults work, *GSA Today*, *14*, 4-10 (September).

Wells, D. L., and K. J. Coppersmith (1994), New empirical relationships among magnitude, rupture length, rupture width, rupture area, and surface displacement, *Bull. Seismol. Soc. Amer.*, *84*, 974-1002.

Table 2. Summary 30-year earthquake probabilities for greater Tokyo

Team Tokyo study (*this study*)	Poisson	Renewal
M≥7.3 within 50 km of Tokyo (1855 Ansei-Edo type)	20 (0-30)	>35
M≥7.9 within 100 km of Tokyo (Taisho or Genroku type)	11 (7-13)	0.5
Combined probability (for I_{JMA}≥6 or PGA≥0.9 *g*)	29 (7-40)	>35
Government study (*Earthquake Research Committee*, 2005)		
M≥6.7 within 80 km of Tokyo (1987 Off-Chiba type)	70	—
M≥7.9 within 100 km of Tokyo (Taisho or Genroku type)	—	≤0.8
Combined probability (for I_{JMA}≥4 or PGA≥0.08-0.10 *g*)	70	

Note that the combined probability in the Government study is equivalent to I_{JMA}≥4, shaking strong enough to awaken sleeping people, but not enough to damage buildings.

Table 3. Kanto M≥7.9 earthquake record

Event age range (calendar year)	Earthquake evidence	Number of earthquakes
AD 1823-2023	historic (1923)	1
AD 1603-1803	historic (1703)	1
AD 990-1220	dated terrace	1
AD 670-760	terrace	1
339 BC-AD 669	no data	any number
530-340 BC	dated terrace	1
889-650 BC	terrace and tsunami	1
1120-890 BC	dated terrace	1
1470-1121 BC	dated terrace	1
1870-1630 BC	dated terrace	1
2300-2000 BC	tsunami	1
2849-2301 BC	undated terrace	1
3050-2850 BC	terrace and tsunami	1
3450-3330 BC	terrace and tsunami	1
3949-3451 BC	undated terrace	1
4060-3950 BC	tsunami	1
4839-4161 BC	undated terrace	1
5020-4840 BC	terrace and tsunami	1

From Shishikura, [*Shishikura*], based on uplifted marine terraces [*Nakata et al.*, 1980; *Shishikura*, 2003] and tsunami deposits [*Fujiwara and Kamataki*, 2003; *Fujiwara et al.*, 1999]. Historic earthquakes are assigned a ±100-yr range roughly equivalent to events dated by ^{14}C. Marine terraces were not formed during the period of rapid sea level rise, and so this time interval can contain any number of earthquakes, including none.

Figure 1. (a) Simplified tectonic map of the Kanto triple junction [*Toda et al.*, 2006], showing the Japan Group and Kashima-Daiichi seamount chains. (b) The Philippine Sea plate is shaded pink where it descends beneath the Eurasian plate. The proposed Kanto fragment (green) lies between the Philippine Sea plate and the underlying Pacific plate. Sites of large historical earthquakes are identified with their tectonic plate element. Two cross-sections through greater Tokyo are shown with 1979-2003 microseismicity in the lower panels.

Figure 2. (a) Peak intensities observed during the past 400 years. Observed intensity distribution for (b) 1923 M=7.9 Kanto (c) 1855 M~7.4 Ansei-Edo, and (d) 1703 M~8.2 Genroku shocks [*Bozkurt et al.*, 2006], together with our inferred seismic sources for these three earthquakes.

Figure 3. (a) Stresses imparted by the 1923 Kanto earthquake [*Nyst et al.*, 2006a] to the surrounding crust may explain the sites of increased and decreased seismicity [*Hamada et al.*, 2001] for the ensuing decades. (b) Seismicity recorded during 1979-2004 in the Kanto region, revealing the concentration of earthquakes in the Kanto seismic corridor. The 23 July 2005 M=6.0 earthquake struck in the North Tokyo Bay cluster, a likely site for the 1855 M~7.3 Ansei-Edo event.

Figure 4. Map of the most probable locations of 1649-1884 earthquakes [*Grunewald*, 2006] superimposed on our tectonic interpretation [*Toda et al.*, 2006]. The Philippine Sea plate is translucent where it subducts beneath the Eurasian plate. In detail, each earthquake is represented by a probability density function for location with magnitude covariance, as shown in Appendix Figure 1.

Figure 5. (a) Slip associated with the subduction of the Philippine Sea plate along he Sagami trough can explain the marine terrace uplift for Taisho (1923-type) and Genroku (1703-type) events, as well as the tsunami that accompanied the 1703 event [*Shishikura et al.*, 2006]. (b) Observed marine terrace ages [*Shishikura*, 2003, 2006]. Event dates are shown in Table 3.

Figure 6. Magnitude-frequency distribution for relocated historical and instrumentally recorded M≥4.5 earthquakes in the Kanto region shown in Figure 5 (a) exhibits a uniform, monotonic distribution with a *b*-value near 1.0. (b) Resulting time-averaged probability as a function of magnitude [*Grunewald*, 2006]. (c-d) Relationships for earthquakes within the Kanto seismic corridor (Figure 3b).

Figure 7. The inferred seismic slip rate (often called the 'slip deficit rate') for the major sources, and their association with larger historic events and historical seismicity, modified from *Nishimura and Sagiya* [2006]. Red sources slip at high rate and are

currently locked, and thus are accumulating tectonic strain to be released in future large earthquakes; white sources have a low slip rate or creep, and so are unlikely to be sites of future large shocks.

Figure 8. The agreement between the inferred rate of seismic moment release [*Grunewald*, 2006] and seismic moment accumulation [*Nishimura and Sagiya*, 2006] ensures that the catalog reasonably represents the long-term seismic behavior of the region. This also increases our confidence in the inferred seismic slip rates in Figure 7.

Figure 9. (a) Probability distribution for the mean inter-event time and aperiodicity for Taisho (1923-type) Sagami trough earthquakes. (b) Resulting time-dependent 30-yr probability. (c) Our 30-yr time-dependent (renewal) and time-averaged (Poisson) probabilities as a function of time, as well as the renewal probability for the Government report, for which an interevent time of 200-400 yr and an aperiodicity of 0.17-0.24 were assumed [*Earthquake Research Committee*, 2005].

Figure 10. (a) The 10,000 intensity observations are collapsed onto one frequency-intensity distribution and fitted to an exponential decay curve. Modern data collected since the 1923 earthquake dominate the low-intensity observations, whereas data from 1600-1900 provide most of the high-intensity data. Fit of the general decay curve to sites in Yokohama with dense (b) and sparse (c) observations [*Bozkurt et al.*, 2006] yield similar probability estimates.

Figure 11. (a) Spatial distribution of the time-averaged 30-year probability of severe shaking (PGA~0.93 *g*), which is consistent with our independent estimate [*Bozkurt et al.*, 2006]. (b) The probability of shaking is correlated with proximity to the plate-boundary faults and to sites of unconsolidated sediments. ISTL is the Itoigawa-Shizuoka Tectonic Line.

Appendix Figure 1. For each earthquake in our 1649-1885 catalog of historic earthquakes [*Grunewald*, 2006], there is a probability function on location (*green contours*) with covariance on magnitude (*red contours*), which arises because of data inadequacy and inconsistency [*Bakun and Wentworth*, 1997]. While the intensity center for the 1856 earthquake corresponds to M=6.8, the magnitude could range over $6.4 \geq M \geq 7.4$ depending on location. In the Monte Carlo sampling, the earthquake location is drawn 1000 times from a random sample consistent with the location function, and the associated magnitude is used in each case.

Table 1. JMA intensity scale and equivalent ground motion parameters

Observations used to assess shaking intensity	JMA Intensity Scale	Estimated Peak Ground Acceleration (at 5-8 Hz)	Estimated Peak Ground Velocity (at 5-8 Hz)	Modified Mercalli Intesnity, MMI
Felt by most people in the building. Some people are frightened.	3	~ 0.02 g	~ 0.02 m/s	V
Many people are frightened. Some people try to escape from danger. Most sleeping people awaken.	4	~ 0.07 g	~ 0.07 m/s	VI
Occasionally, less earthquake-resistant houses suffer damage to walls and pillars.	5 lower	~ 0.26 g	~ 0.26 m/s	VII-VIII
Occasionally, less earthquake-resistant houses suffer heavy damage to walls and pillars, and lean.	5 upper			
Occasionally, less earthquake-resistant houses collapse and even walls and pillars of highly earthquake-resistant houses are damaged.	6 lower	~ 0.95 g	~ 0.93 m/s	IX-X
Many less earthquake-resistant houses collapse. In some cases, even walls and pillars of highly earthquake-resistant houses are heavily damaged.	6 upper			
Occasionally, even highly earthquake-resistant houses are severely damaged and lean.	7	~ 3.4 g	~ 3.3 m/s	XI-XII
Source: *Japan Meteorological Agency* (2004)		*Karim and & Yamazaki* (2002)		

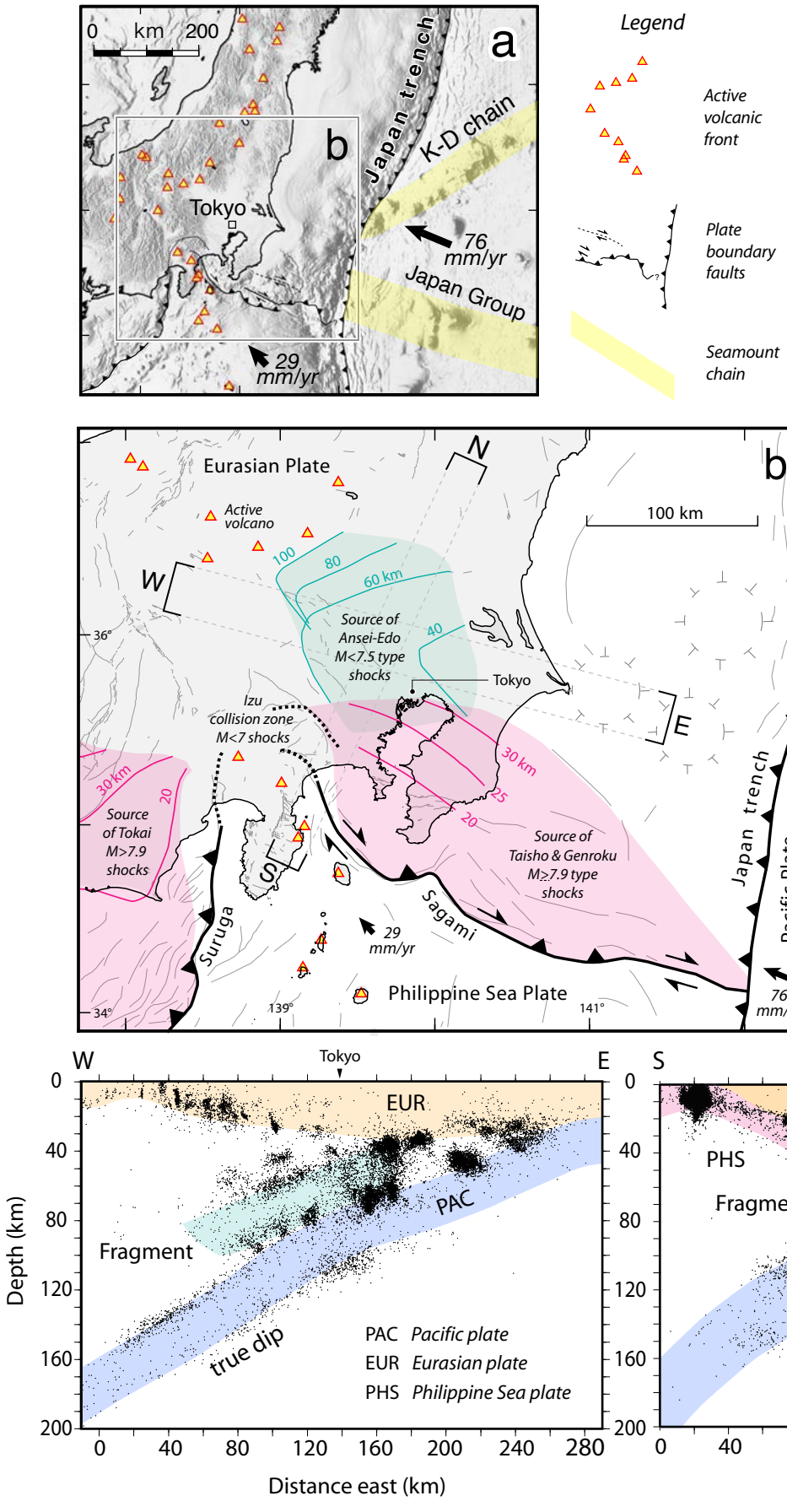

Figure 1
Stein et al

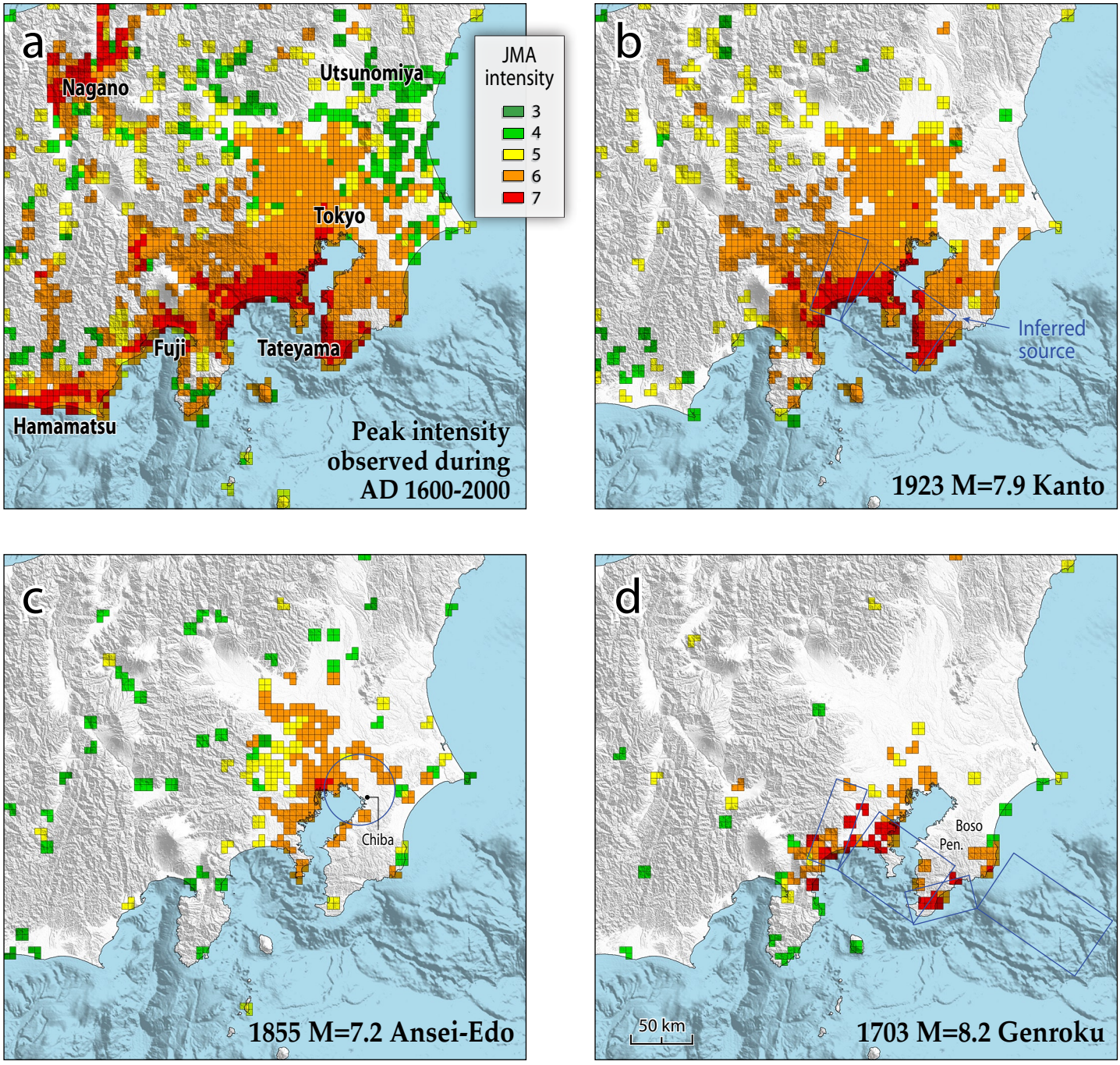

Figure 2
Stein et al

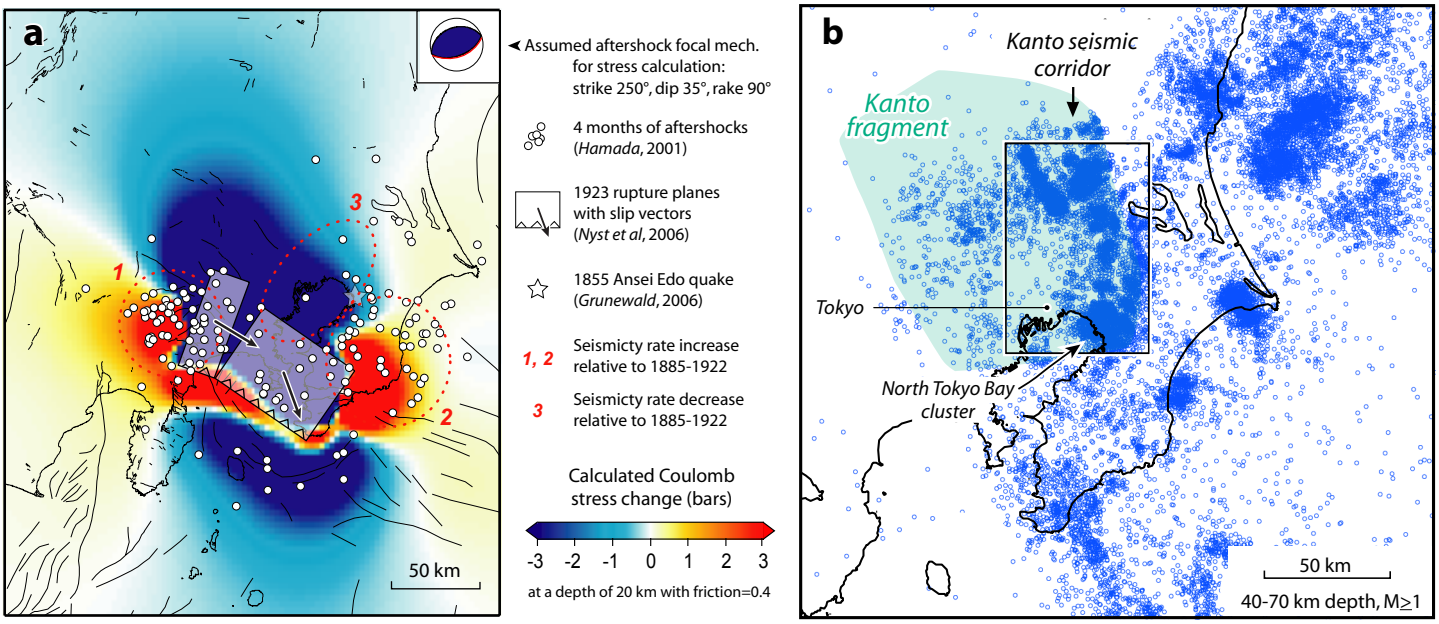

Fig. 3
Stein et al

Grunewald (2005)

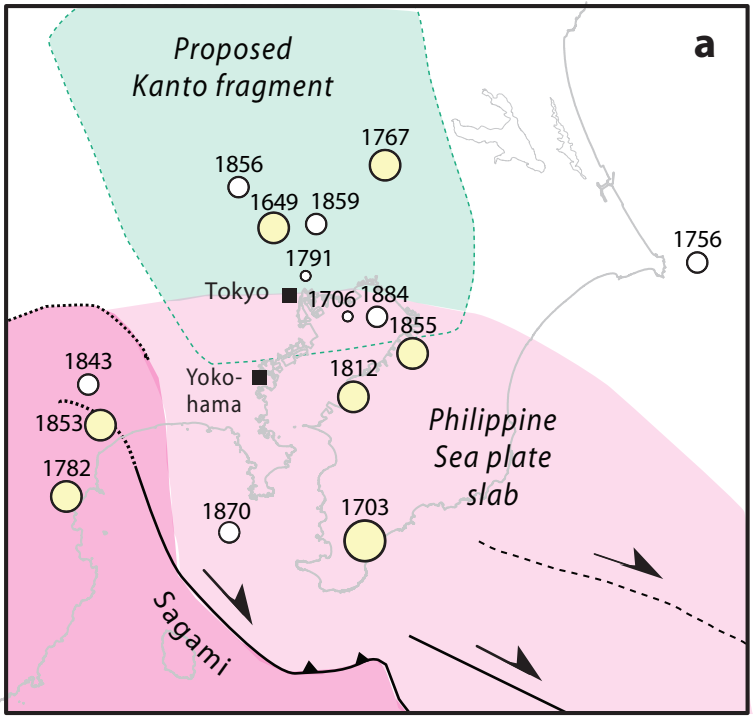

Usami (2003)

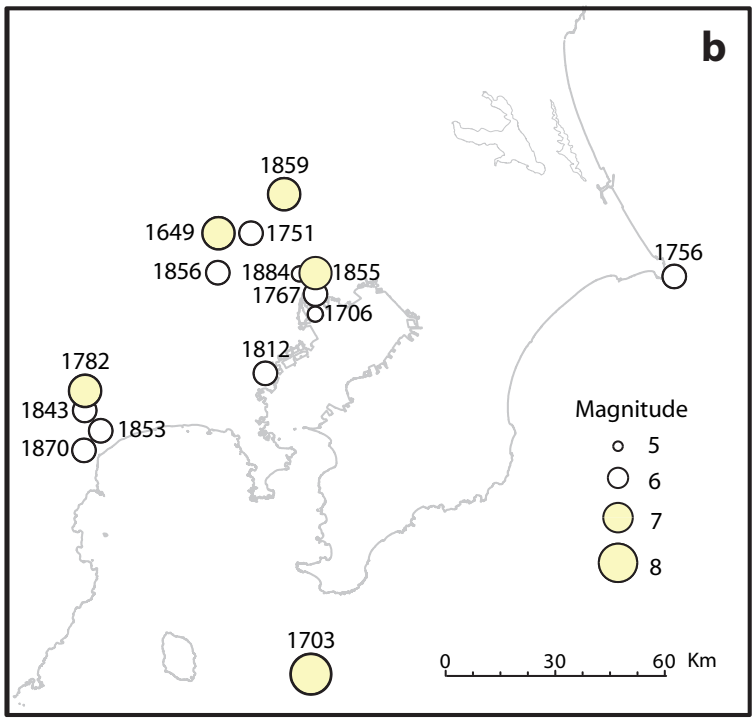

Figure 4
Stein et al

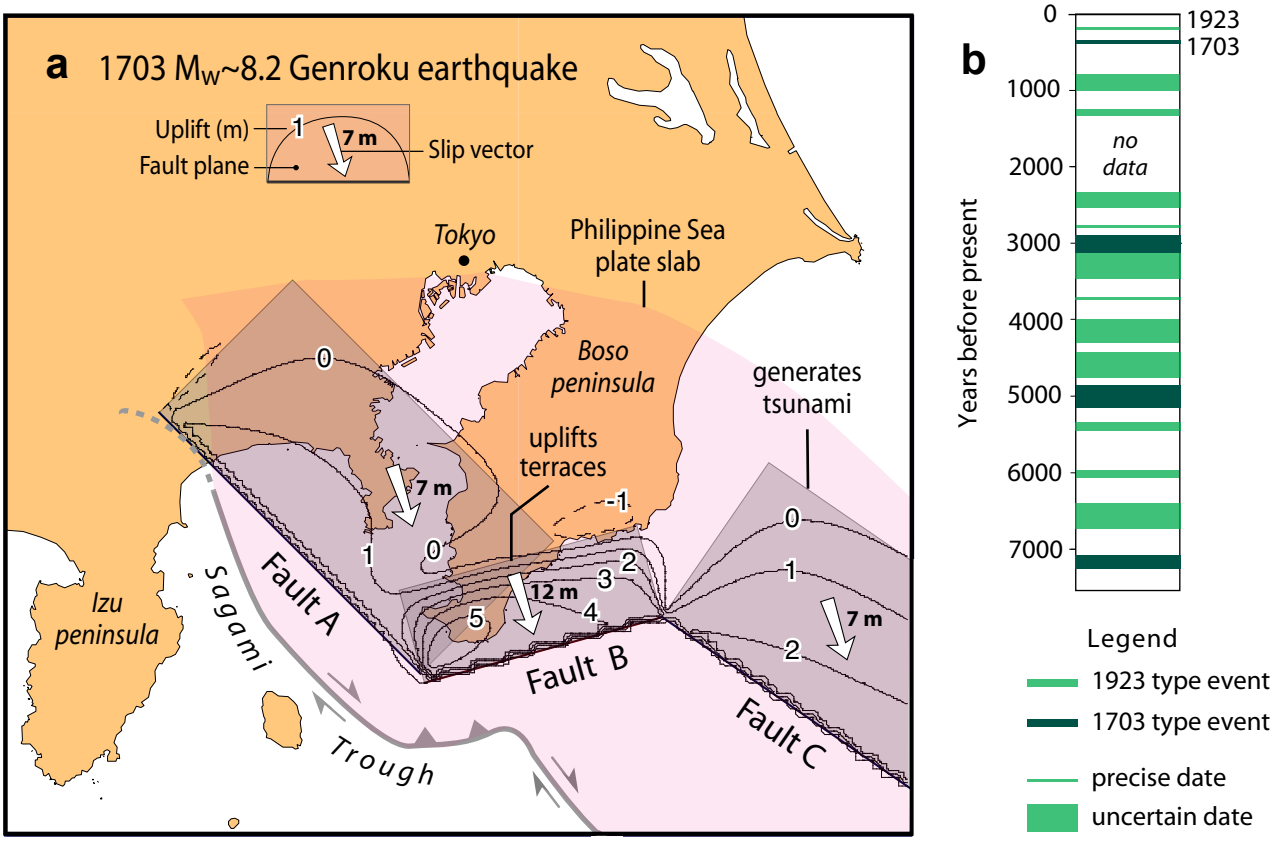

Figure 5
Stein et al

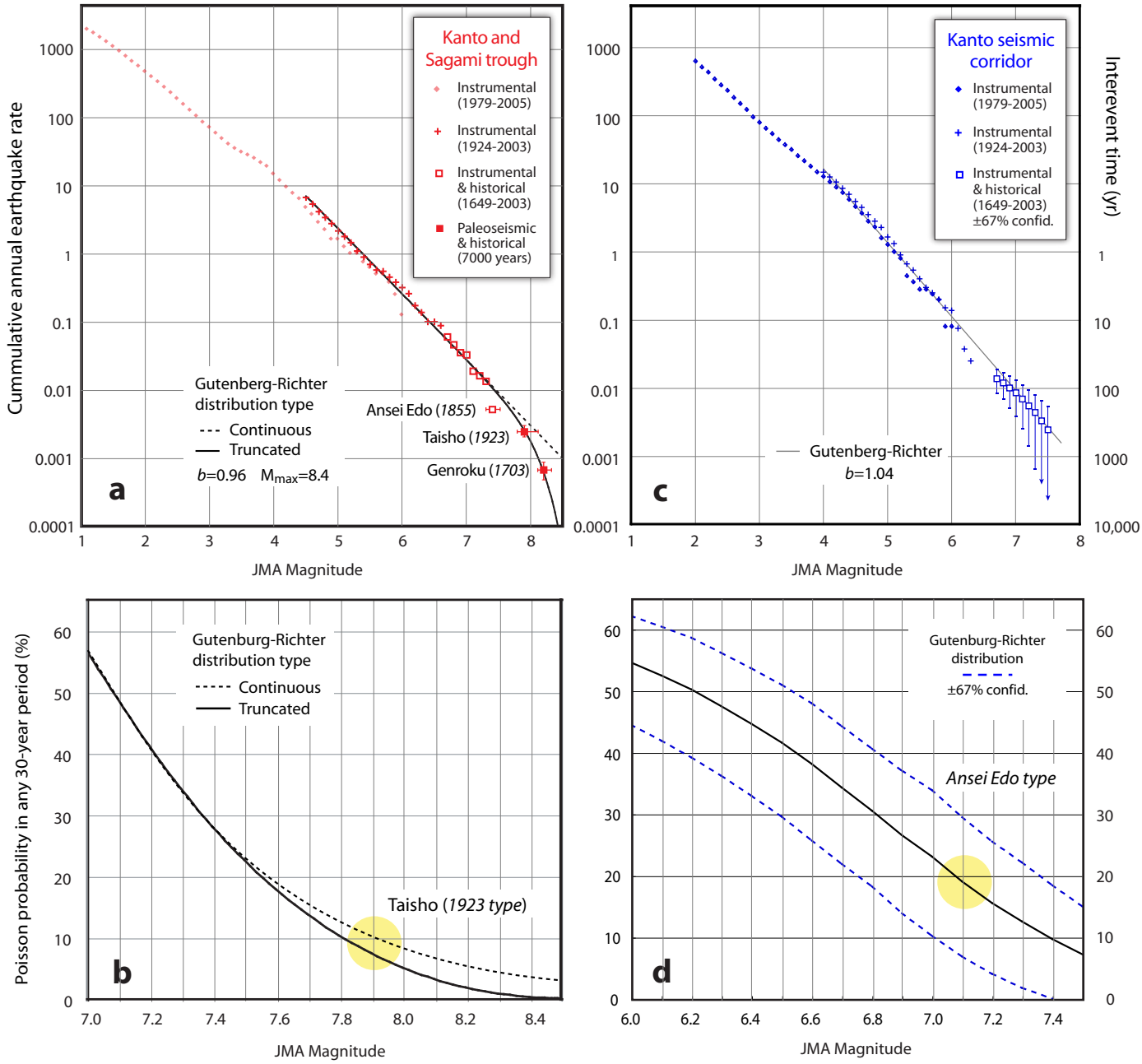

Figure 6
Stein et al

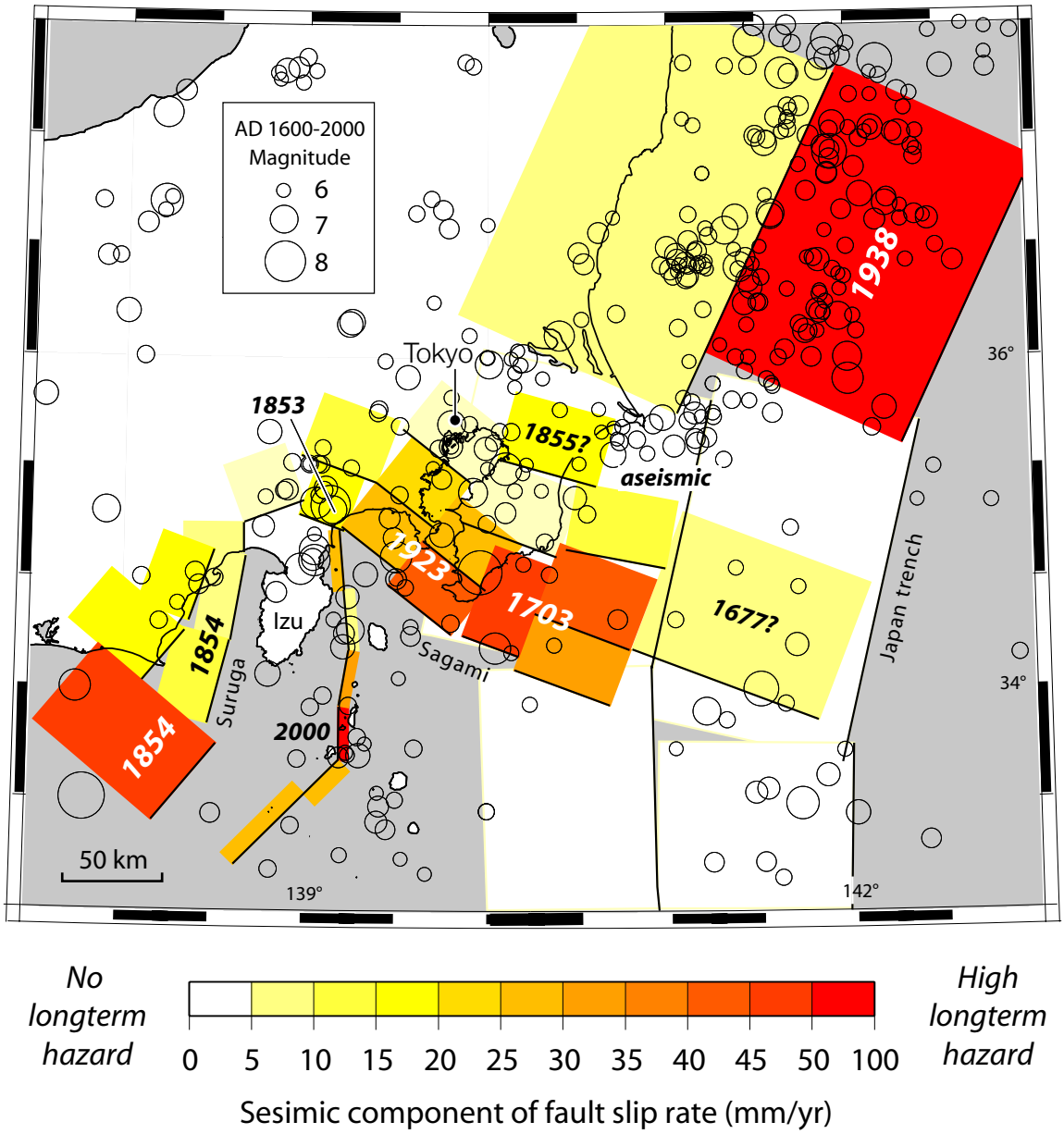

Figure 7
Stein et al

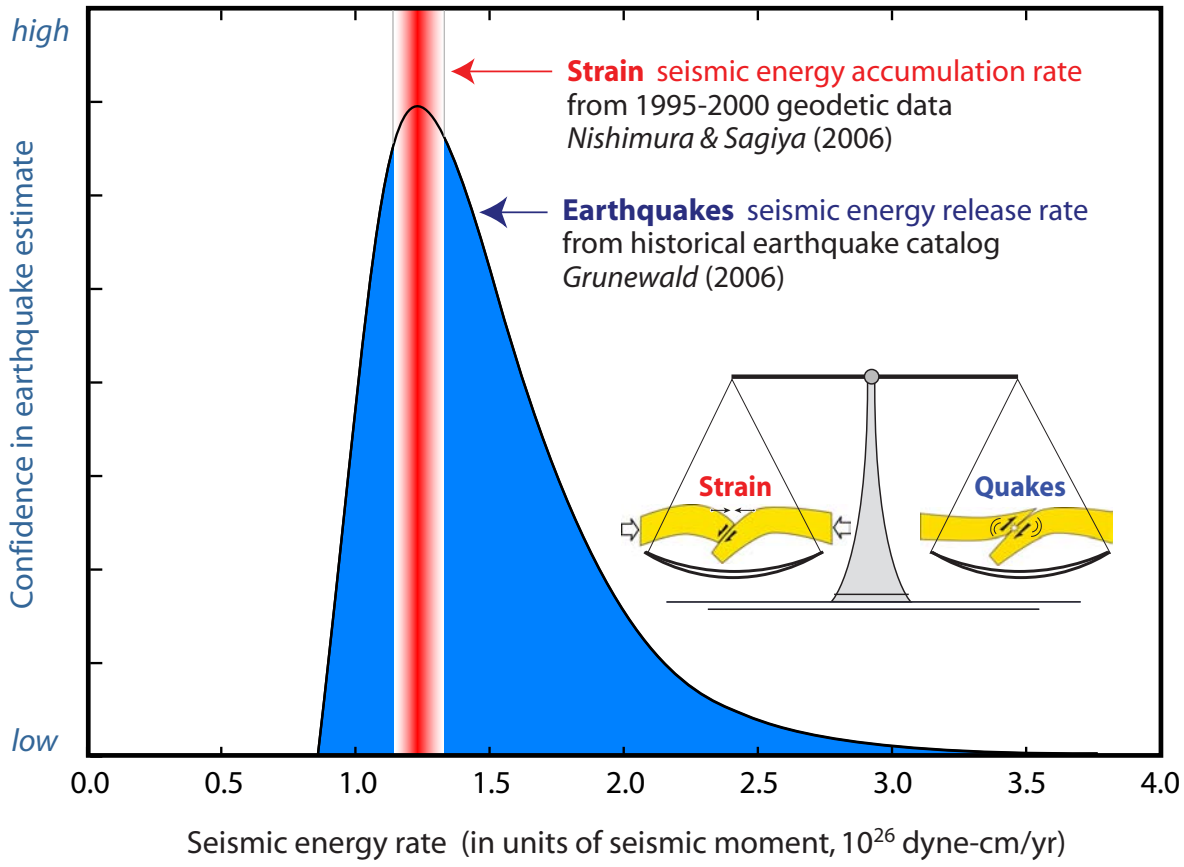

Figure 8
Stein et al

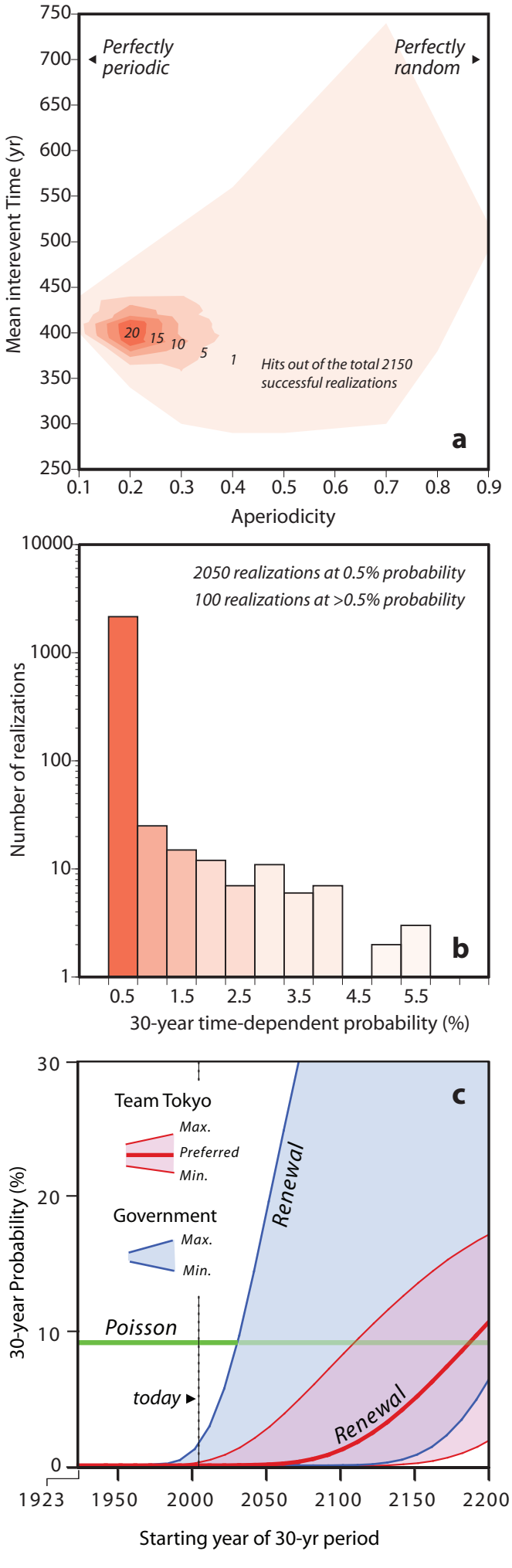

Figure 9
Stein et al

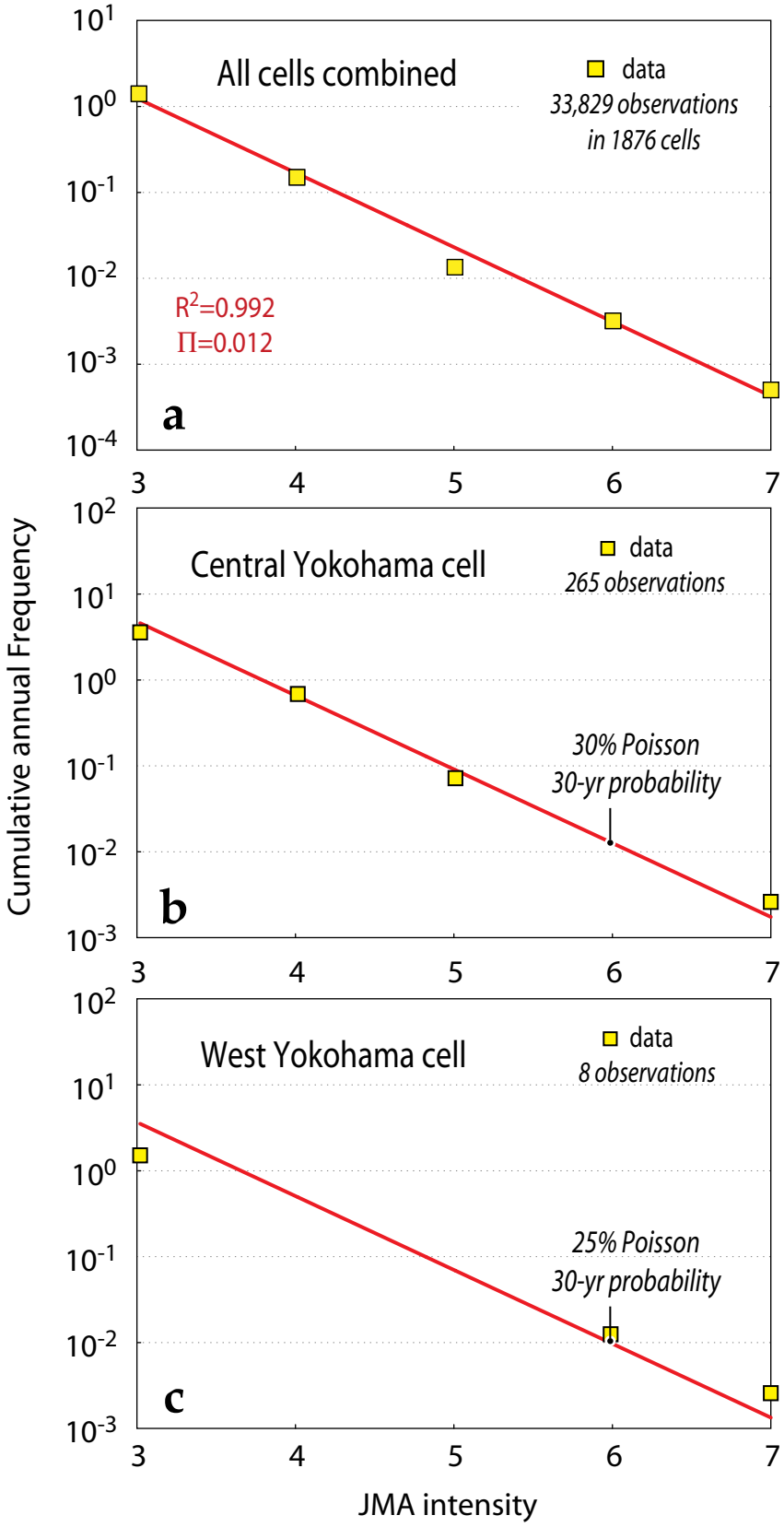

Figure 10
Stein et al

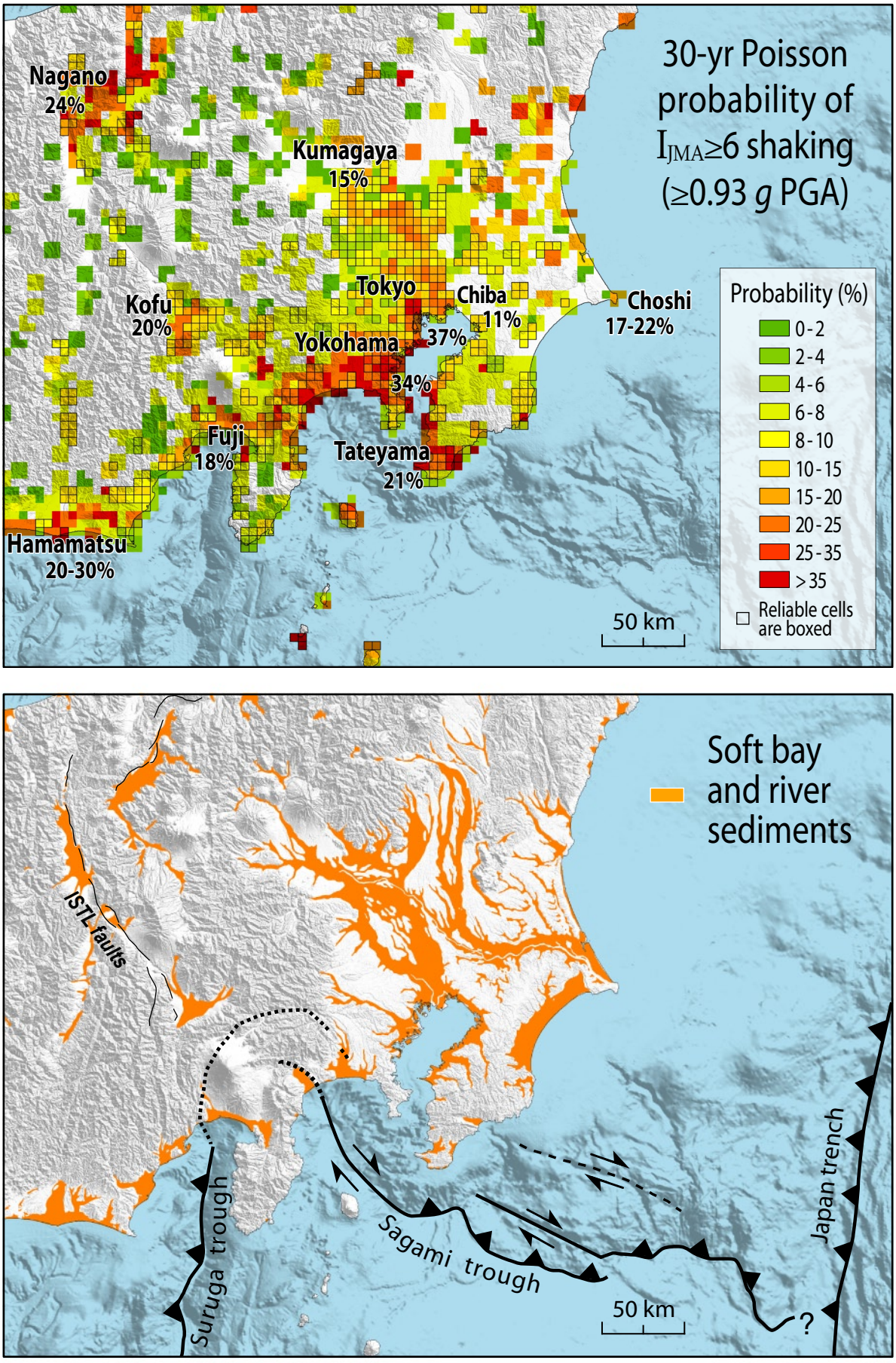

Figure 11
Stein et al

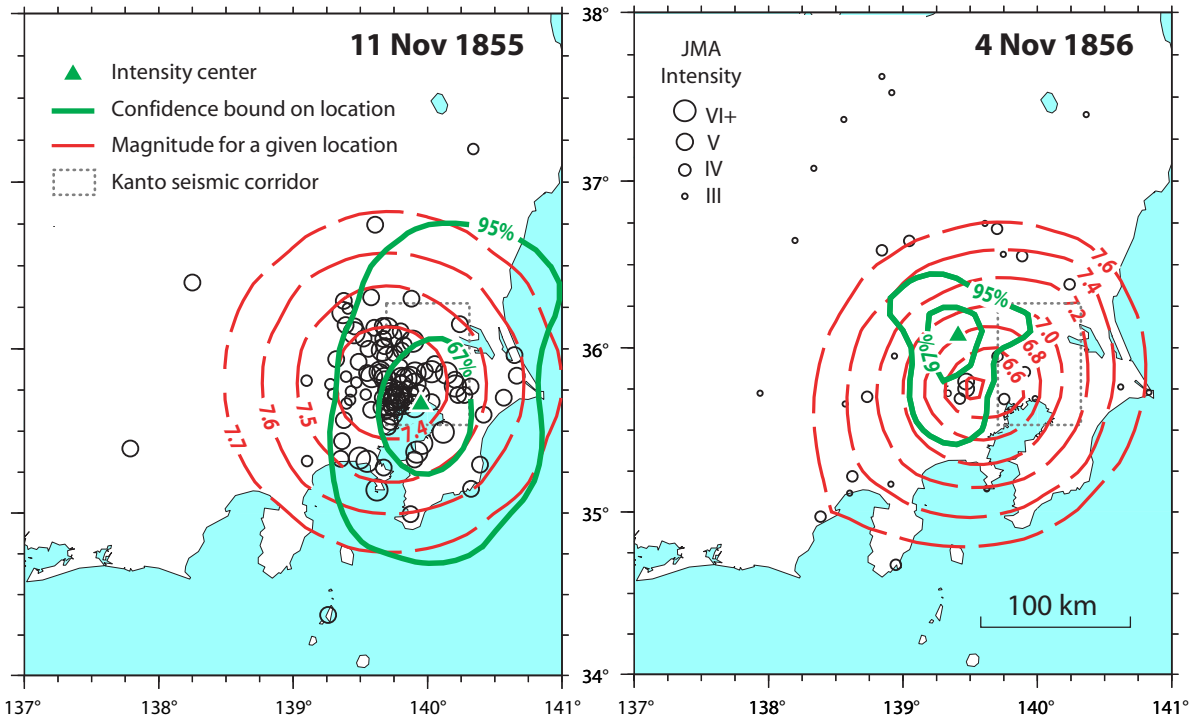

Appendix Figure 1
Stein et al